Recent Advances in the Theory and Simulation Of Pellet Ablation and Fast Fuel Relocation In Tokamaks

P.B. Parks,[1] L.R. Baylor,[2] R. Ishizaki,[3] S.C. Jardin,[4] and R. Samtaney[4]

[1]General Atomics, P.O. Box 85608, San Diego, California 92186-5608, USA
[2]Oak Ridge National Laboratory, Oak Ridge, Tennessee 37381, USA
[3]National Institute for Fusion Science, Toki, Japan
[4]Princeton Plasma Physics Laboratory, Princeton, New Jersey

20th IAEA Fusion Energy Conference
Vilamoura, Portugal
November 1–6, 2004

DIII-D NATIONAL FUSION FACILITY SAN DIEGO

GENERAL ATOMICS

Outline of Topics

- Pellet Ablation
  - New 2-D Eulerian code **CAP** treats multi-phase pellet-cloud dynamics. [Phys of Plasmas **11**, 4064 (2004)]. Magnetic field interaction now partially included.
  - Ionized cloud pushes B-field away forming a diamagnetic cocoon around pellet. Diverts plasma energy flux around pellet, prolonging its lifetime.
- ∇B induced cloud drift using **PRL** code (GA-A24807 submitted to Phys Rev Lett)
  - Included plasma pressure profile variations on drifting cloudlet
  - Showed that the M ~1 parallel ablation flow furthers cloudlet penetration
  - Elucidated the effect of rotational transform on cloudlet drift
  - Discovered how magnetic shear causes cloudlet "mass shedding" and dispersal
  - Generalized theory to include arbitrary poloidal angle of pellet entry
- 3-D MHD simulations of ∇B cloud drift using Adaptive Mesh Reduction code **AMR**
  - Preliminary results verify that pellet cloud drifts in large-*R* direction

CAP code: Numerical Approach and Assumptions

- Geometry
  - Axisymmetric cylindrical coordinates (r, θ, z) with θ ignorable, and background (undisturbed) magnetic field B_∞ parallel to z axis.
  - Magnetic field → B_r, B_z, flow velocity → v_r, v_z , current J_θ , electric field E_θ
- Rectangular (r,z) Computational Box
  - Ideally conducting wall boundary at $r_{wall} \approx 20\ r_{pell}$
  - Reflecting (outflow) boundary conditions at end faces $z_{end} \approx \pm 20\ r_{pell}$
- Some Physical Assumptions Made:
  - Solve magnetic flux equation with simple Ohms law, $E_\theta = - v \times B + J_\theta / \sigma_\perp$.
  - Use step-function heat flux to pellet (realistic pellet entry has gradual increase).
  - Artificially high electrical resistivity η_∞ in background plasma is needed to eliminate significant currents and J×B forces, which are "continually erased" by fast magnetosonic adjustments on the slow cloud evolution time scale.

Magnetic Field Force Limits Transverse Cloud Dimension

Density ρ Contours $\log_{10}$ kg/m^3
at 0.4 μs

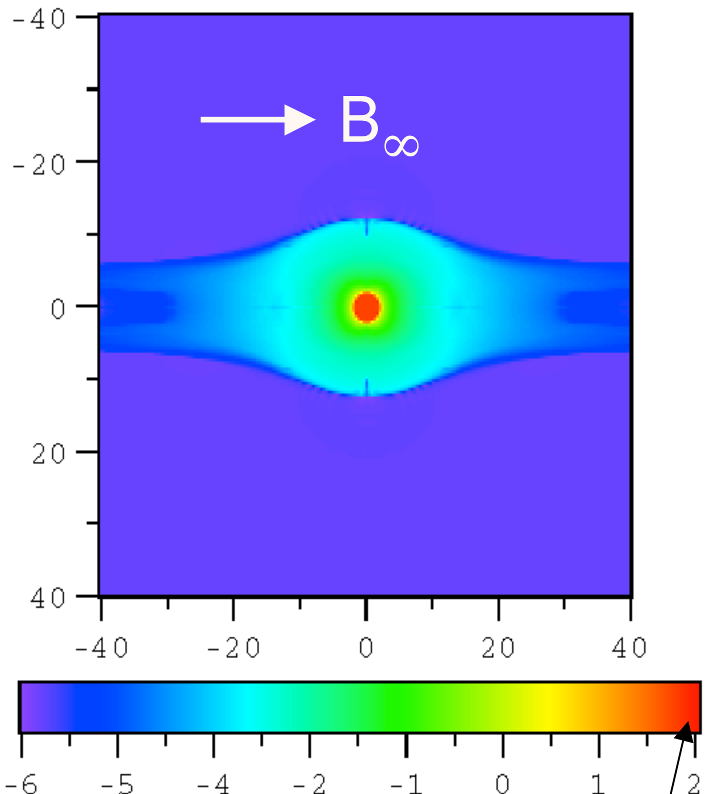

Pellet density 200 kg/m^3

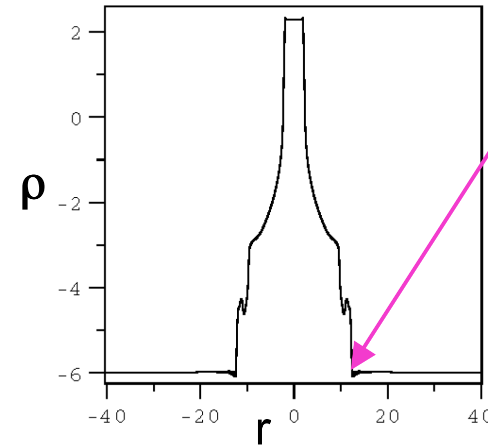

Transverse expansion of cloud limited to $r_\perp$ = 10 mm (5 r_{pell}) by JxB force.

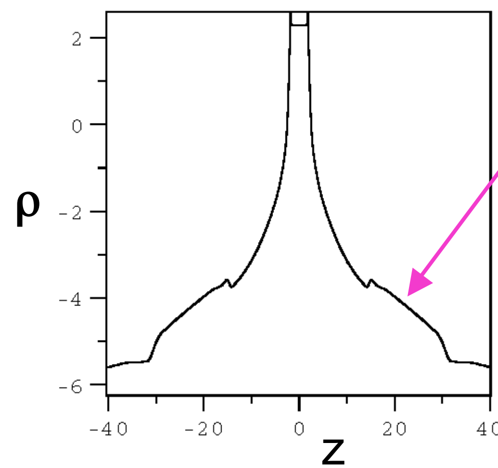

Parallel expansion is free, but not yet fully developed after only 0.4 μs

β~1 Diamagnetic Cavity Can Divert Heat Flux Around Pellet

Contours of B^2 at 0.4μs

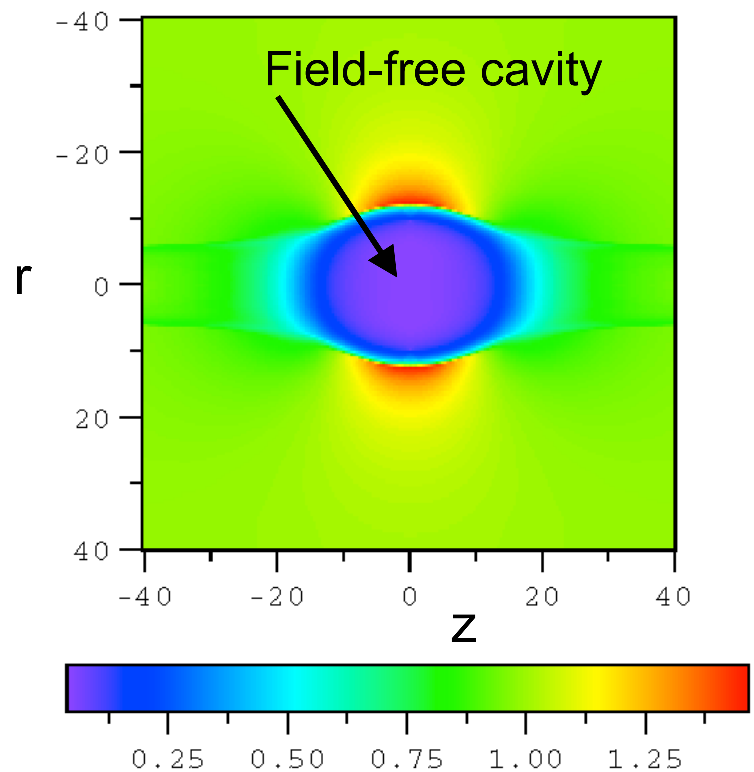

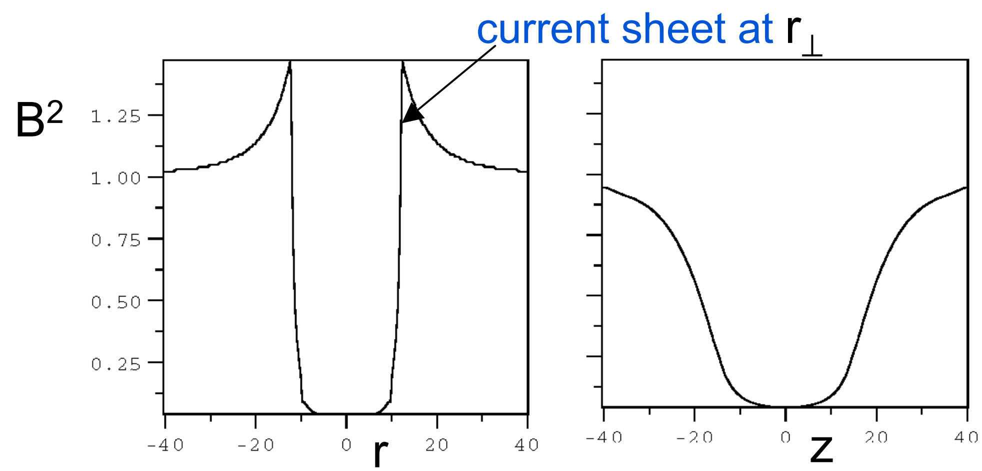

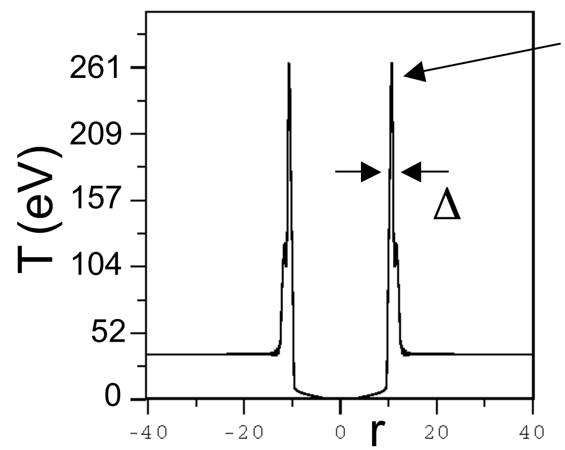

Hot ring and **current sheet** formed as rarefied ablation front is compressed against magnetic field by impact with the dense flow behind front.

Hot ring can potentially maintain field-free cavity over the long skin time $\tau_{skin} = \mu_0 \sigma_\perp \Delta\, r_\perp \sim 60\ \mu s > r_\perp / v \sim 1\ \mu s$. **Distorted field lines can potentially divert heat flux around pellet, reducing ablation rate.**

Basic Ingredients of ∇B Cloud Drift & Fast Fuel Relocation Model

- Ordering and scales
  - Cloudlet is like a strongly localized cylindrical pressure perturbation

    $\nabla_\perp \sim 1/r_c \ll 1/R,\ 1/a,\qquad \delta \equiv r_c/qL(t) \sim v_c/qc_s \ll 1$ (key expansion parameter)

    v_c = E/B drift velocity ~ 10^3–10^4 m/s, c_s = cloudlet sound speed ~ 10^4–10^5 m/s,

- Transverse force balance (no fast time-scale magnetosonic waves $v_c \ll c_{A\infty}$)

$$0 \cong \nabla_\perp(\delta p + B_\infty \delta B/\mu_0) + O(r_c/R) \longrightarrow \delta p = -B_\infty \delta B/\mu_0$$

$\delta p = p_c - p_\infty$ $\quad p_c$ = cloud pressure, "∞"= ambient plasma quantity

"excess pressure" is source of curvature drive

- Parallel expansion flows relax pressure perturbation δp
  - Pressure Relaxation Lagrangian (PRL) code (Parks, PoP 2000)
  - End boundary condition applied on a drifting cloudet

$$p_c(z = L) = p_\infty(\rho = \rho_c) \qquad \rho_c(t) = \text{ minor radius of cloud centroid}$$

Pressure Profile Variation Works Against Penetration

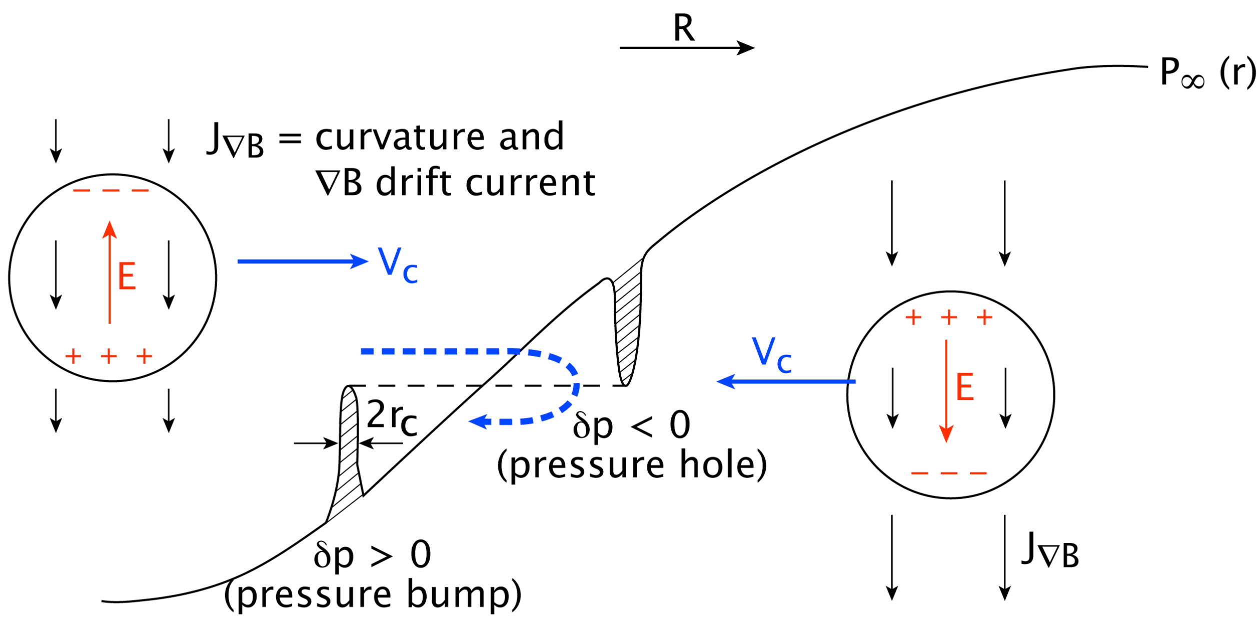

- A local positive pressure bump ($\delta p > 0$) is necessary to start the inward drift V_c. In doing so the pressure bump could change to a pressure hole ($\delta p < 0$), causing drift reversal. Pellet penetration well past edge pedestal region seems to be necessary for good cloud penetration.

GENERAL ATOMICS

Beginning Point: Peturbed Parallel Vorticity Equation

- Evolution of plasma vorticity [Hazeltine,1992]

$$\frac{\hat{b}}{B}\cdot\nabla\times mn\frac{d\vec{v}}{dt}=(\vec{B}\cdot\nabla)\frac{J_{||}}{B}-\frac{(\hat{b}\times\vec{\kappa})\cdot\nabla_{\perp}B^2}{\mu_0 B}$$

where $\hat{b}=\vec{B}/B,\ \kappa=\hat{b}\cdot\nabla\hat{b}$ (curvature), $B^2=B_{\infty}^2+2B_{\infty}\delta B,\ J_{||}=J_{||\infty}+\delta J_{||}.$

- Perturbed result with substitution $-2\delta p=2B_{\infty}\delta B/\mu_0$

$$\frac{\hat{b}}{B}\cdot\nabla\times mn\frac{d\vec{v}}{dt}=(\vec{B}\cdot\nabla)\frac{\delta J_{||}}{B}+\frac{2(\hat{b}\times\vec{\kappa})\cdot\nabla_{\perp}\delta p}{B}$$

(Inertial Forces) (Alfven Waves) (Curvature Drive)

- Inertial term becomes exactly

Coriolis force — Centrifugal force

$$\frac{d\vec{v}}{dt}=\hat{b}\left(\frac{\partial v_{||}}{\partial t}+v_{||}\frac{\partial v_{||}}{\partial s}+\vec{v}_{\perp}\cdot\nabla v_{||}-v_{||}\vec{\kappa}\cdot\vec{v}_{\perp}\right)+v_{||}(\nabla\times\hat{b})_{||}\hat{b}\times\vec{v}_{\perp}-v_{||}\hat{b}\times\nabla\times\vec{v}_{\perp}+v_{||}^2\vec{\kappa}+\frac{D\vec{v}_{\perp}}{Dt}$$

$$\frac{\hat{b}}{B}\cdot\nabla\times mn(\ ) \rightarrow O(\delta)\ \text{neglect}$$

$$\frac{D}{Dt}=\frac{\partial}{\partial t}+\vec{v}_{\perp}\cdot\nabla$$

Vorticity Equation Yields Electrostatic Potential Φ and Cross-Field Cloud and Plasma Drifts Near Cloud

$$\vec{v}_\perp = \hat{b} \times \frac{\nabla \Phi}{B} \longrightarrow \nabla_\perp \cdot \left(\frac{mn}{B^2} \frac{D \nabla_\perp \Phi}{Dt} \right) = (\vec{B} \cdot \nabla) \frac{\delta J_\parallel}{B} + \frac{(\hat{b} \times \vec{\kappa}) \cdot \nabla_\perp (2\delta p + mn v_\parallel^2)}{B}$$

Centrifugal force driving term operates, even after $\delta p \rightarrow 0$

- Tokamak coordinate system (ρ, χ, ϕ) for poloidal plane (ρ, χ) variations

$$\hat{b} \times \vec{\kappa} = -(\hat{\chi} \cos\chi + \hat{\rho} \sin\chi)/R$$

- Helical magnetic-field-line-following (MFLF) coordinate system (x,y) or (r,ϑ) for local cloud variables: $\nabla_\perp (2\delta p + mn v_\parallel^2) = \partial / \partial r (2\delta p + mn v_\parallel^2) \hat{r}$

$$\boxed{(\hat{b} \times \vec{\kappa}) \cdot \hat{r} = \frac{-1}{R} \left(\cos\chi \sin\vartheta + \sin\chi \cos\vartheta \right)}$$

How Toroidicity modifies curvature drive

$$\chi(z,t) = \chi_0 + \int_0^t \frac{v_\chi(t')}{\rho(t')} dt' \pm \frac{z}{qR}$$

q = safety factor

χ_0 = pellet launch angle

$\chi_0 + \int_0^t \frac{v_\chi(t')}{\rho(t')} dt' = \chi_c(t)$

Position of cloud centroid (x = y = z = 0)

Helical Magnetic-Field-Line Following (MFLF) Coordinates $\vec{x}$ Suitable for Local Cloud Variables

Illustrates transformation between circular high-aspect-ratio tokamak coordinates $\vec{\rho}$ and cloud coordinates $\vec{x}$

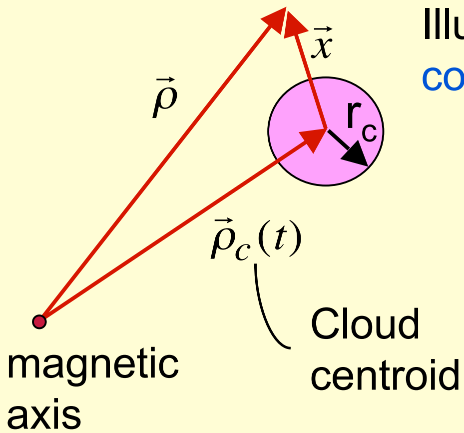

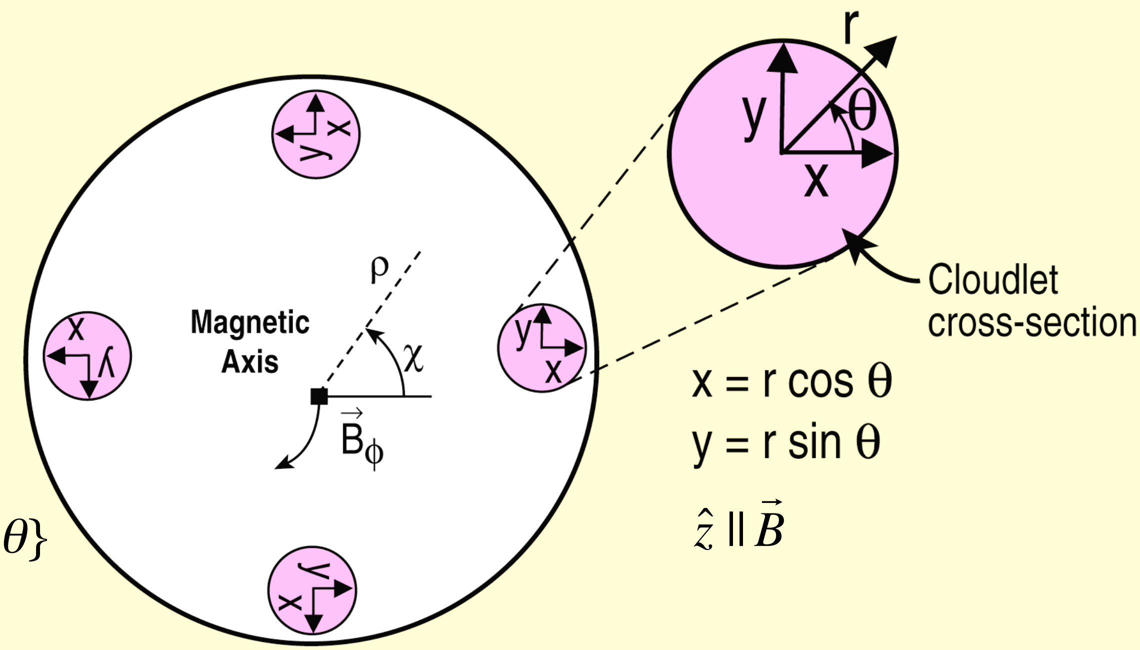

$$\vec{\rho} = \vec{\rho}_c(t) + \vec{x},$$
$$\vec{\rho} = \{\rho,\chi\}, \quad \vec{x} = \{x,y\} \text{ or } \{r,\theta\}$$

$x = r\cos\theta$

$y = r\sin\theta$

$\hat{z} \parallel \vec{B}$

- Local cross-field coordinates (x, y) affixed to cross-section of cloud: x = const, y = const identify a field line. Due to rotational transform, the coordinates rotate counter-clockwise with longitudinal distance z

$\nabla_{\parallel}\Phi \approx 0$ so $\Phi(x,y)$ is frozen to B-field lines in cloud

Field-Line-Average Along Cloudlet Length

- Match parallel end-current $\delta J_{//}$ with the current carried off by shear Alfven wave excited by motion in ambient plasma $E_{||} = -ik_{||}\Phi + i\omega A_{||} = 0$ (Parks, PoP 2000)

$$\nabla_\perp \cdot \vec{\Gamma} = S(r,\vartheta) \equiv \frac{2}{BR}\delta(r-r_c)\left[\sin\vartheta\cos\chi_c(t) + \cos\vartheta\sin\chi_c(t)\right]\Psi(t)$$

Assumed flat radial cloud profiles

$$\vec{\Gamma} = \frac{m\tau}{B^2}\frac{D\nabla_\perp\Phi}{Dt} + \frac{\nabla_\perp\Phi}{\mu_0 c_{A\infty}}$$

Shear Alfven wave part

Line-averaged inertial (polarization) drift current

$$\tau = \int_{-L_c}^{L_c} n dz, \quad \tau_{cloud} \sim 10^3 \tau_{plasma}$$

- Drive integral folds parallel (z) variations with changing direction of ∇B-drift current

$$\Psi(t) = \int_0^{L_c(t)} \left[p_c(z,t)[1 + M_c^2(z,t)/2] - p_\infty(t)\right]\cos(z/qR)dz$$

- Boundary condition on electrostatic potential at "infinity"

$$\Phi(\vec{x},t) \rightarrow -E_{\rho\infty}[\rho_c(t)]x$$

Radial (ρ) electric field in tokamak at cloud centroid

Nondimensional Drift Equations Use Parameters of 1-D Ablation Channel Flow Formed around Solid Pellet

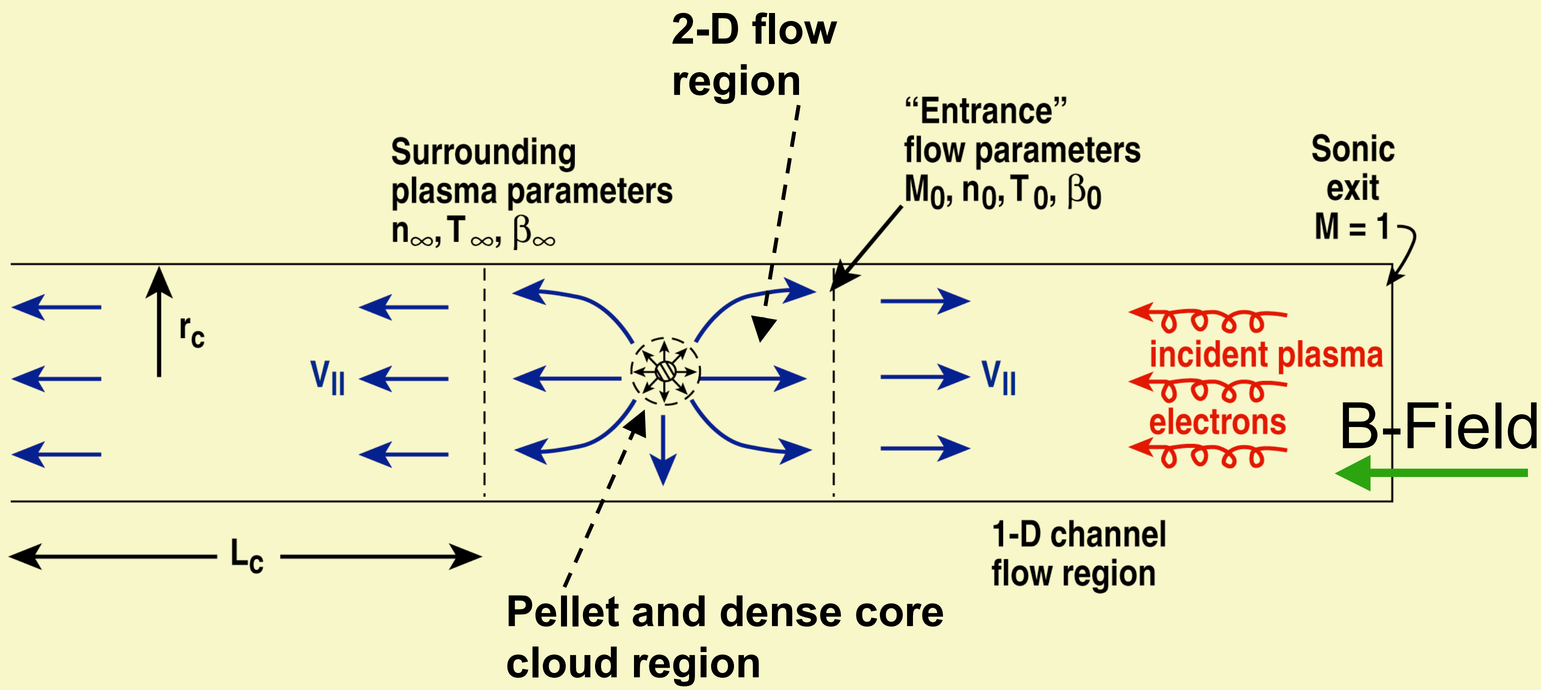

- $\tilde{t} = \dfrac{t}{(L_c / c_0)}$, $\tilde{\rho}_c = \rho_c / a$, $u_\rho = \dfrac{\mathrm{v}_\rho}{c_0}$, $u_\chi = \dfrac{\mathrm{v}_\chi}{c_0}$, $u_E = \dfrac{\mathrm{v}_{\perp\infty}^{E\times B}}{c_0}$, $c_0^2 = \dfrac{2T_0}{m}$

- Normalized curvature drive integral $\tilde{\Psi} = \dfrac{\Psi(t)}{p_0 L_c}$, $p_0 = 2 n_0 T_0$

Non-dimensional Drift Equations

- Radial and Poloidal velocities and coordinates $\rho_c(\tilde{t}), \chi_c(\tilde{t})$ are coupled

$$\tilde{M}(\tilde{t})\frac{du_\rho}{d\tilde{t}} = -\nu_{drag}u_\rho + g\tilde{\Psi}(\tilde{t})\cos\chi_c(\tilde{t}) + w\tilde{M}(\tilde{t})\frac{u_\chi^2}{\tilde{\rho}_c(\tilde{t})}$$

Centripetal force

$$M(\tilde{t})\frac{du_\chi}{d\tilde{t}} = -\nu_{drag}[u_\chi - u_{\perp\infty}^{E\times B}(\tilde{\rho}_c)] - g\tilde{\Psi}(\tilde{t})\sin\chi_c(\tilde{t}) - w\tilde{M}(\tilde{t})\frac{u_\rho u_\chi}{\tilde{\rho}_c(\tilde{t})}$$

Coriolis force

Alfven drag coefficient *Normalized Curvature* *Normalized Cloud mass*

$$\nu_{drag} = \left(\frac{L_c}{L_{skid}}\right), \qquad g = \frac{2L_c}{\bar{\tau}R}, \quad w = \frac{L_c}{a}, \quad \tilde{M} = \frac{M(t)}{M(0)}$$

"Skidding Length" $= r_{gi}n_0e\mu_0c_{A\infty}L_c/(2B)$ $\quad N.Brennen\ J.Geo.Res.\ 1991$

$P.Parks\ NF\ \ 1991$

- Cloud mass loss $\frac{d\tilde{M}}{d\tilde{t}}$ comes from “Mass Shedding”

Magnetic Shear Leads to “Mass Shedding”

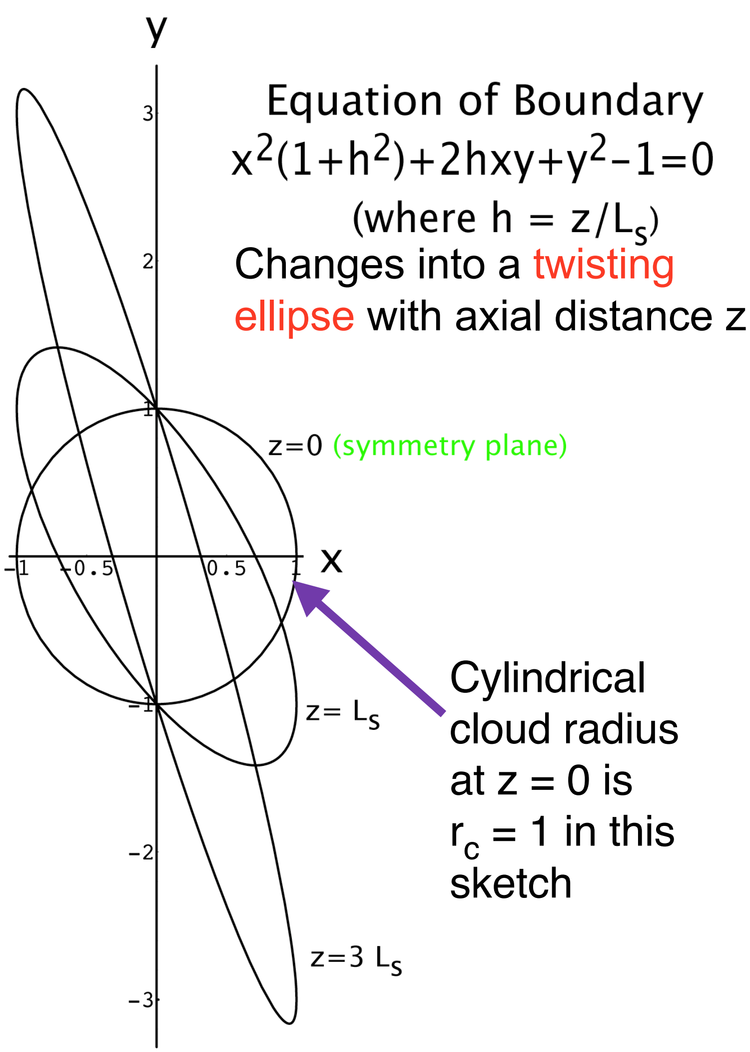

- Elliptical compression and rotation re-orients polarization charges
- Leads to small differential poloidal drift increasing with z
- Limits axial extent of drift response
- “Mass shedding” results

$L_s = qR/\hat{s}$ magnetic shear length

$\hat{s} = \frac{\rho}{q}\frac{dq}{d\rho}$ shear parameter

Phenomenological Model Of Mass Shedding

- Natural "twisted basis" coordinates for a flux tube cloud filament, where $x_* =$ const, $y_* =$ const identifies a field line

$$x_* = x \ , \quad y_* = y - \frac{xz}{L_s}$$

- Transform internal cloud electrostatic potential solution without shear $\Phi^0(x,y)$ to an approximate one with shear by simple mapping $\Phi_{in}^0(x,y) \to \Phi_{in}(x_*,y_*)$

- For this representation $\frac{\partial \Phi_{in}}{\partial x} = \frac{\partial \Phi_{in}}{\partial x_*} - \frac{\partial \Phi_{in}}{\partial y_*}\frac{z}{L_s} \ , \quad \frac{\partial \Phi_{in}}{\partial y} = \frac{\partial \Phi_{in}}{\partial y_*}$

$$\longrightarrow \quad \vec{\mathrm{v}}_{in} = \mathrm{v}_\rho^0 \hat{x} + \mathrm{v}_\chi^0 \hat{y} + \mathrm{v}_\rho^0 \frac{z}{L_s}\hat{y}$$

Cloud acquires small differential poloidal drift ($z < L(t) << L_s$)

- The coherent cloud drift is effectively limited in longitudinal extent when

$$2r_c = \int_0^{t_S(z_0)} \frac{\mathrm{v}_\rho^0(t) z(z_0,t)\,dt}{L_s[\rho_c(t)]}$$

Shedding time $t_S(z_0)$ for fluid element with Lagrangian coordinate z_0

- Mass loss rate $\frac{d\tilde{M}}{dt} = \frac{d\tilde{M}}{dz_0}\frac{dz_0}{dt_S}$ decreases with weaker shear (larger L_s)

Pressure Relaxation Lagrangian (PRL) Code Solves Coupled Drift and Parallel Dynamics for a Series of Cloudlets

- The PRL code uses the pellet size and plasma parameters at each point along the ablation track determined by PELLET code [Houlberg, 1988] to initialize the cloudlet parameters using model of Parks et al PoP 2000.
- The experimental plasma profiles are used by PRL to calculate the subsequent cloudlet pressure relaxation and drift velocity.
- The deposition profiles from each cloudlet are summed, yielding a net Δn profile.
- Parallel Mach number M for a single cloudlet (DIII-D 98796) is shown as a function of normalized time and Lagrangian coordinate $\tilde{z}$.

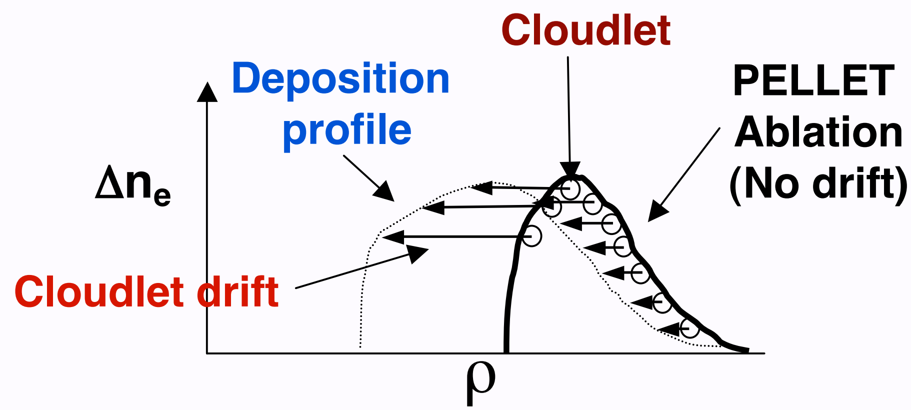

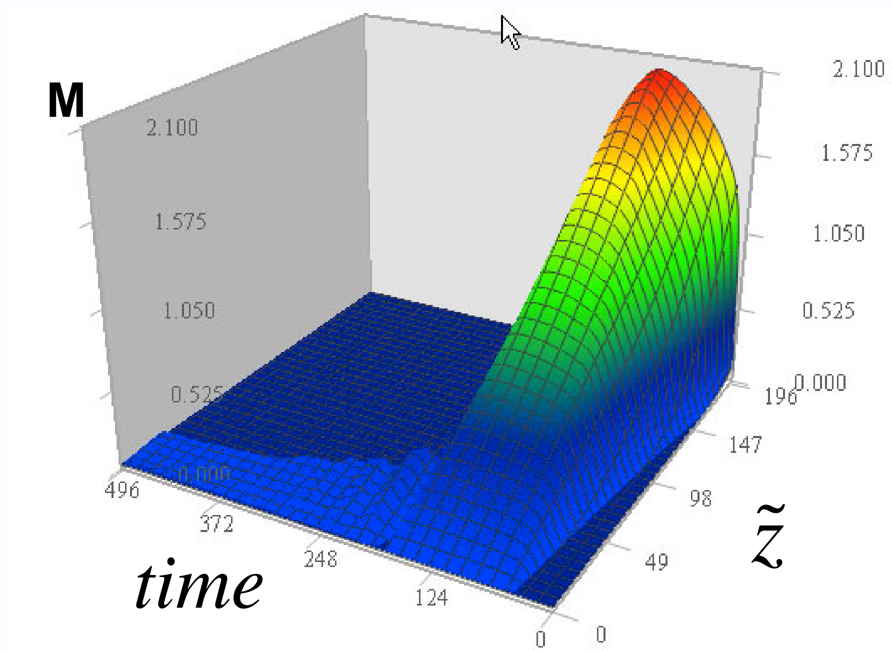

Simulation of Temperature and Pressure Inside Cloudlet with Mass Shedding

Cloudlet temperature evolution

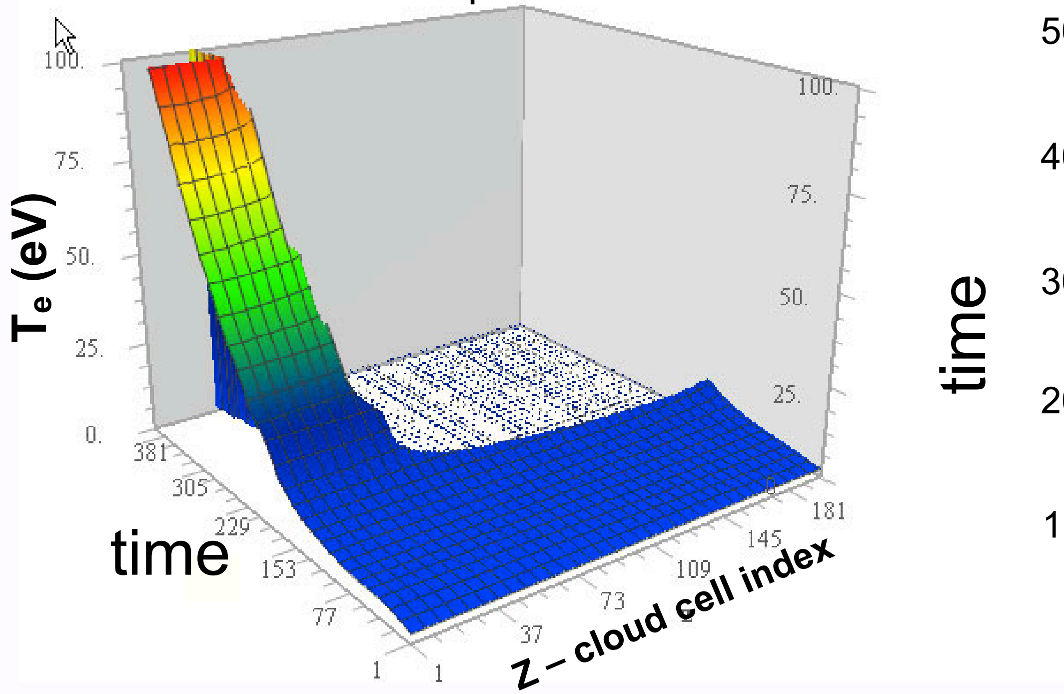

Cloudlet pressure evolution

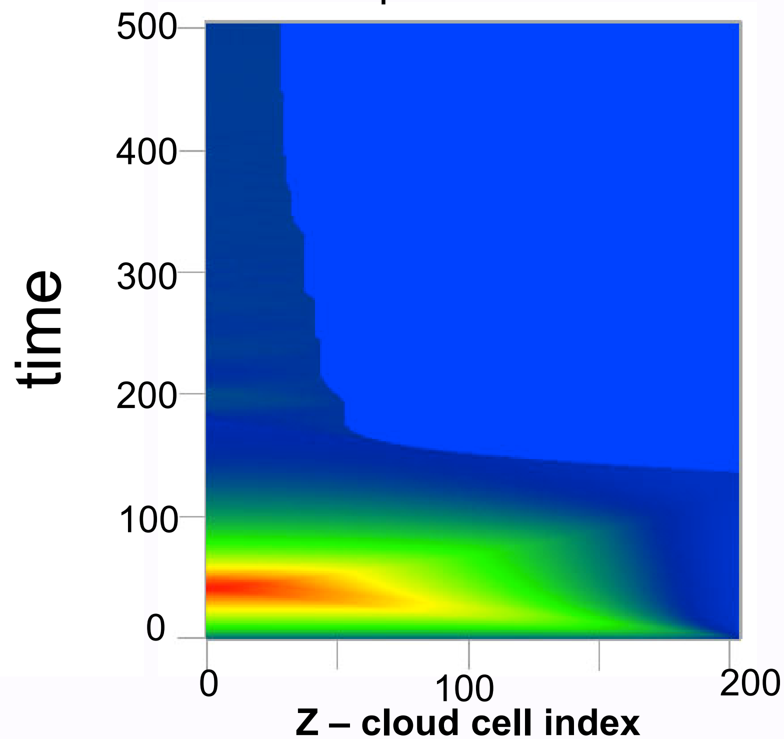

- Temperature and pressure evolution for typical cloudlet in DIII-D 98796. The cloudlet mass shedding can be seen by the reduced number of cells that starts at $t_{cycle} = 150$ (3 μsec). The cloudlet pressure builds quickly then decays as the density decays due to expansion along the field lines.

Theory and DIII-D Experiments Agree

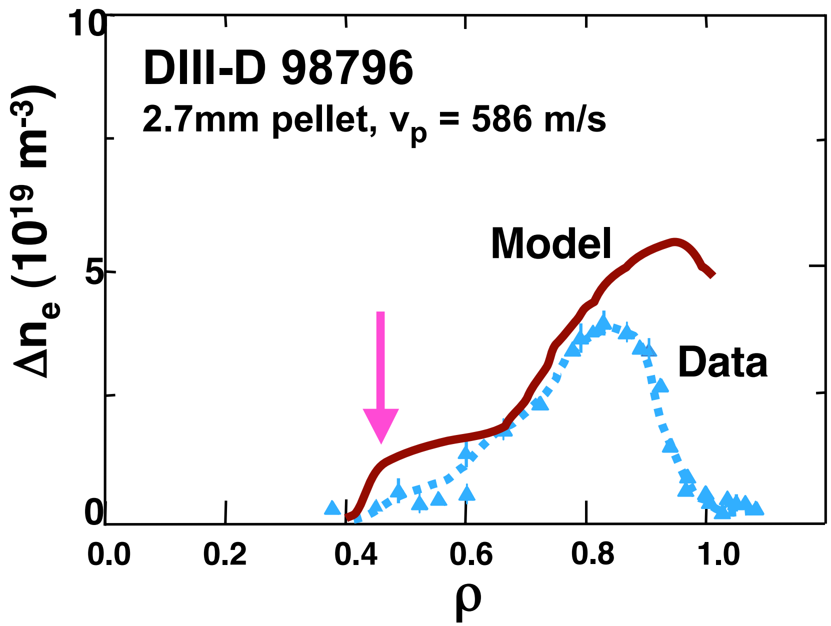

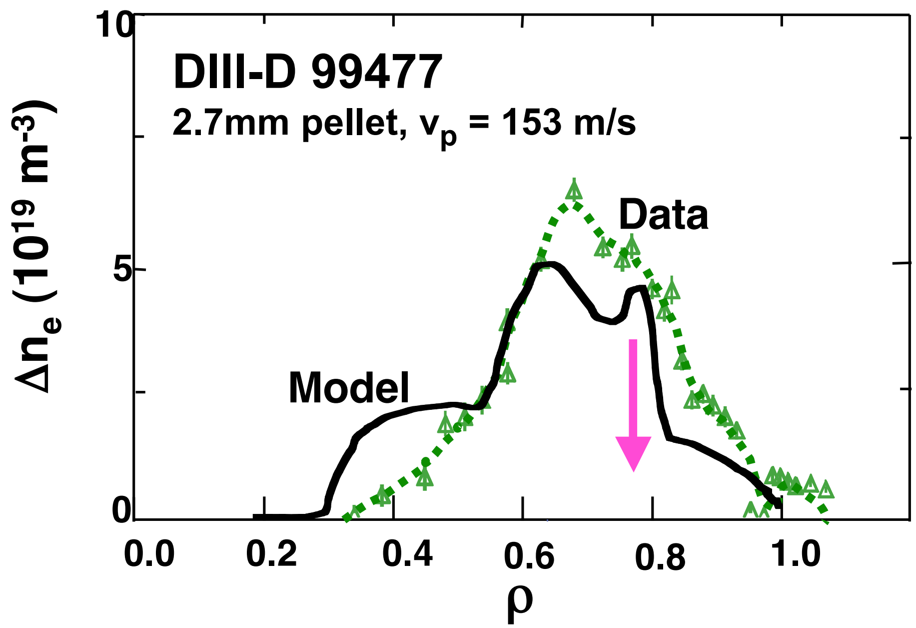

- Vertical arrows indicate pellet burnout point.
- Fueling efficiency for inside launch is much better (even with slower pellets)

outside launch η_{theory} = 66% , η_{exp} = 46% (discrepancy due to strong ELM)

inside launch η_{theory} = 100% , η_{exp} = 92% (discrepancy due to weak ELM)

Parameters for the Following ITER Calculations

$a = 2\ \text{m},\ R_0 = 6\,\text{m},\ n_e = 10^{14}\,\text{cm}^{-3}\text{(flat)},\ \ T_e =$ (P.B. Snyder profile NF 2004)

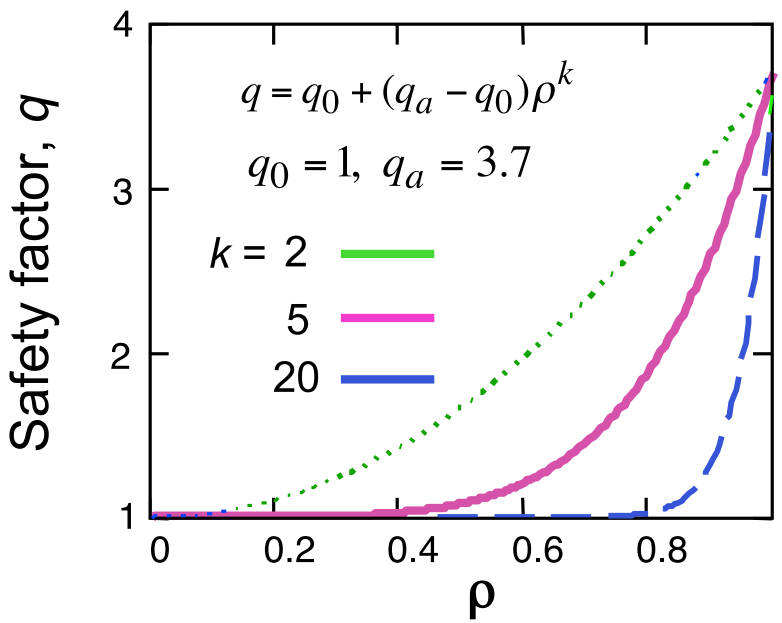

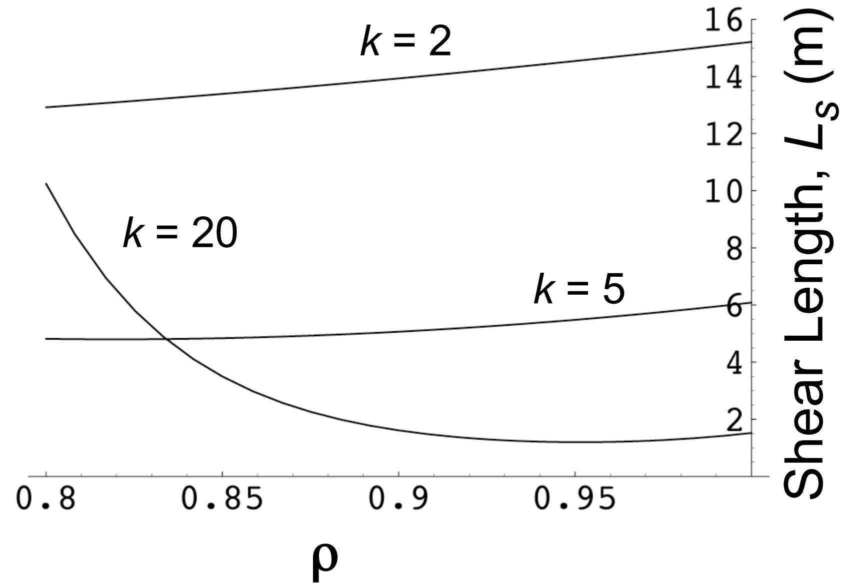

• In ITER, pellets ablate near plasma edge, forming ~ 10-20 cloudlets. We find that the cloudlet drift distance is sensitive to L_s near edge

How ITER Deposition Changes with q-Profile

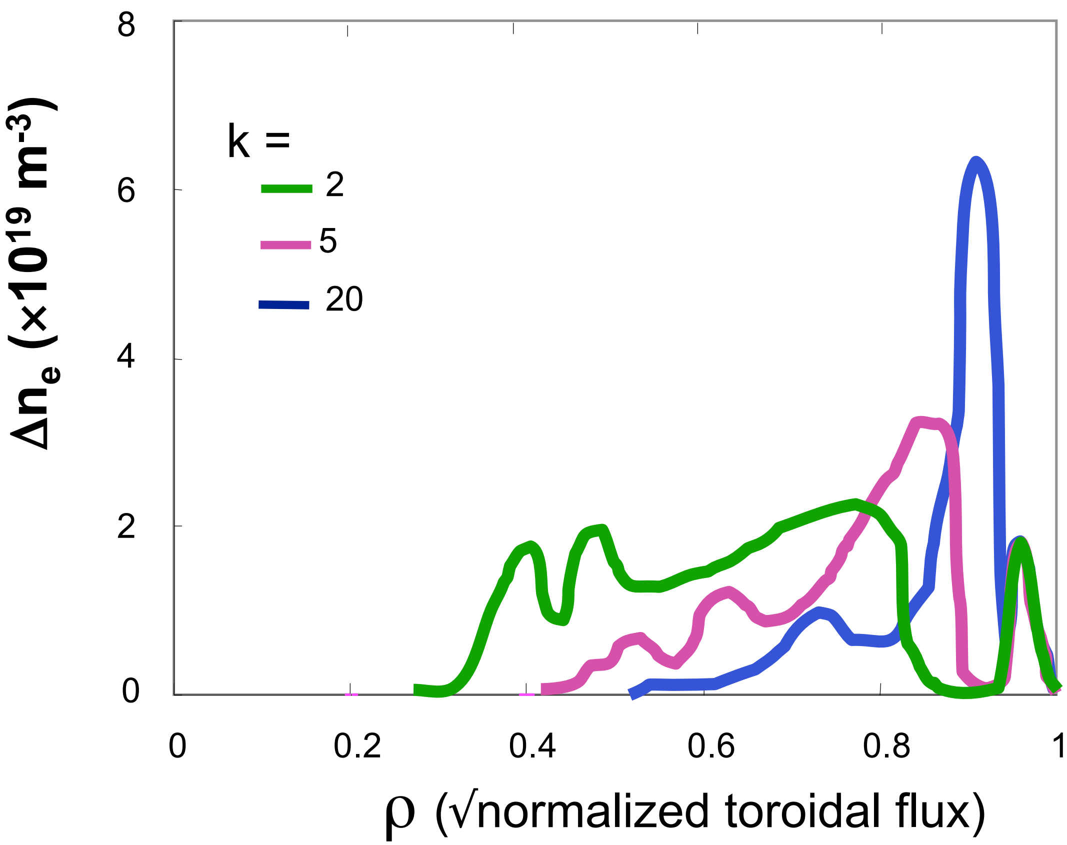

6 mm D2 pellet
T_0 = 20 keV
T_{ped} = 4 keV
v_p = 300 m/s
Inner Wall (45 deg)
Launch:

—The strong shear case near the edge (k = 20) leads to early mass shedding and less penetration.

ITER Deposition Profile Insensitive to T_{ped} for Finite Δ_{ped}

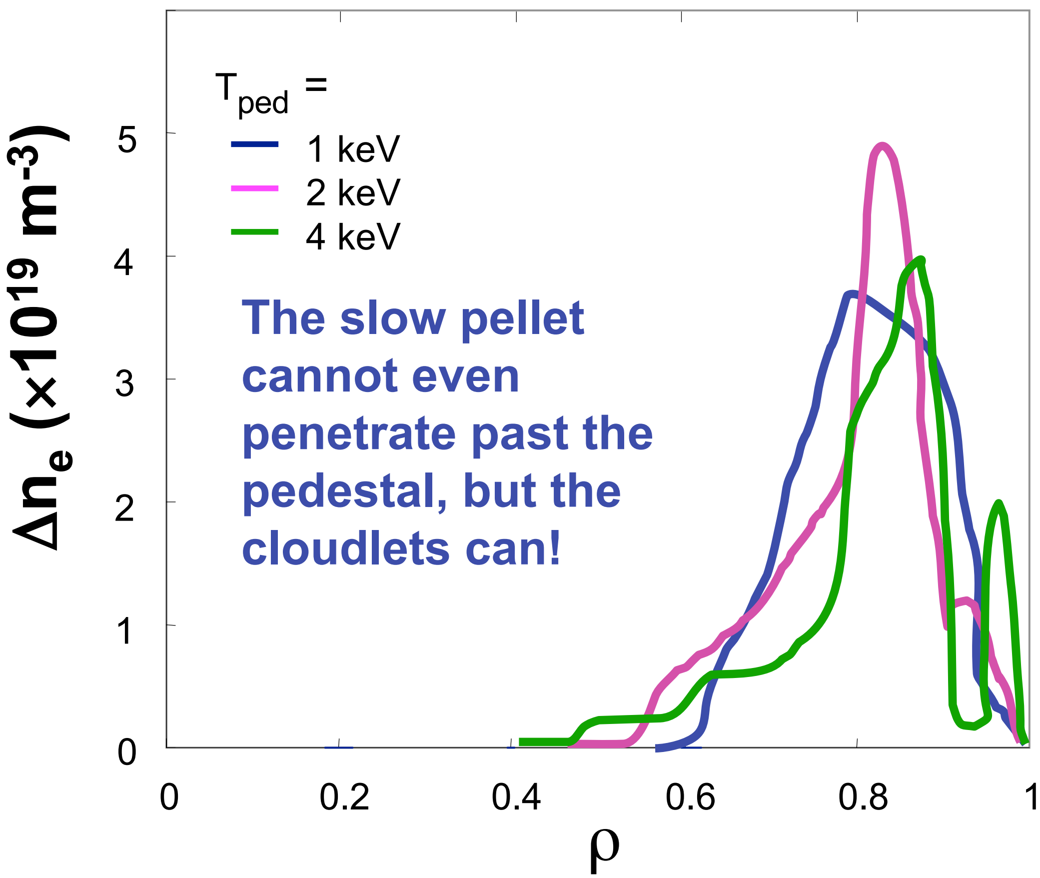

Δ_{ped} = 8 cm
T_0 = 20 keV
6 mm D_2 pellet, v_{pell} = 300 m/s,
45 deg below midplane entry
q-profile with *k* = 5

- As T_{ped} increases, the temperature where pellet burns out T_{burn} increases as $T_{burn} \sim T_{ped}^{3/8}$, forming higher cloudlet pressures…However penetration is more shallow, so the cloudlets have to drift further up the pedestal. These **two effects almost cancel.** → **Deposition remains fairly constant.**

Oak Ridge National Laboratory

General Atomics

ITER Deposition Improves with T_{ped} for zero Δ_{ped}

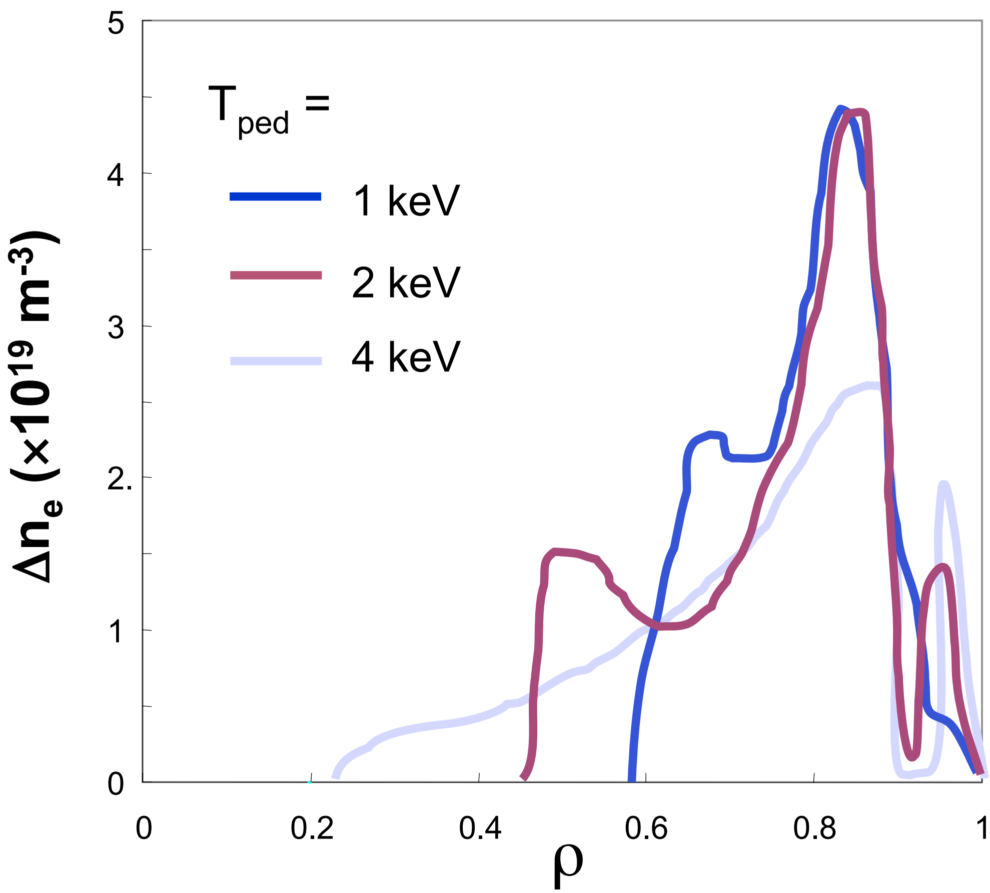

T_0 = 10 keV, 6 mm D_2 pellet, v_{pell} = 300 m/s, 45 deg below midplane entry

➢Higher T_{ped}, leads to deeper fuel penetration

→ makes higher pressure cloudlets which drift further

ITER Inner Wall (45 deg) Deposition Versus Pellet Speed

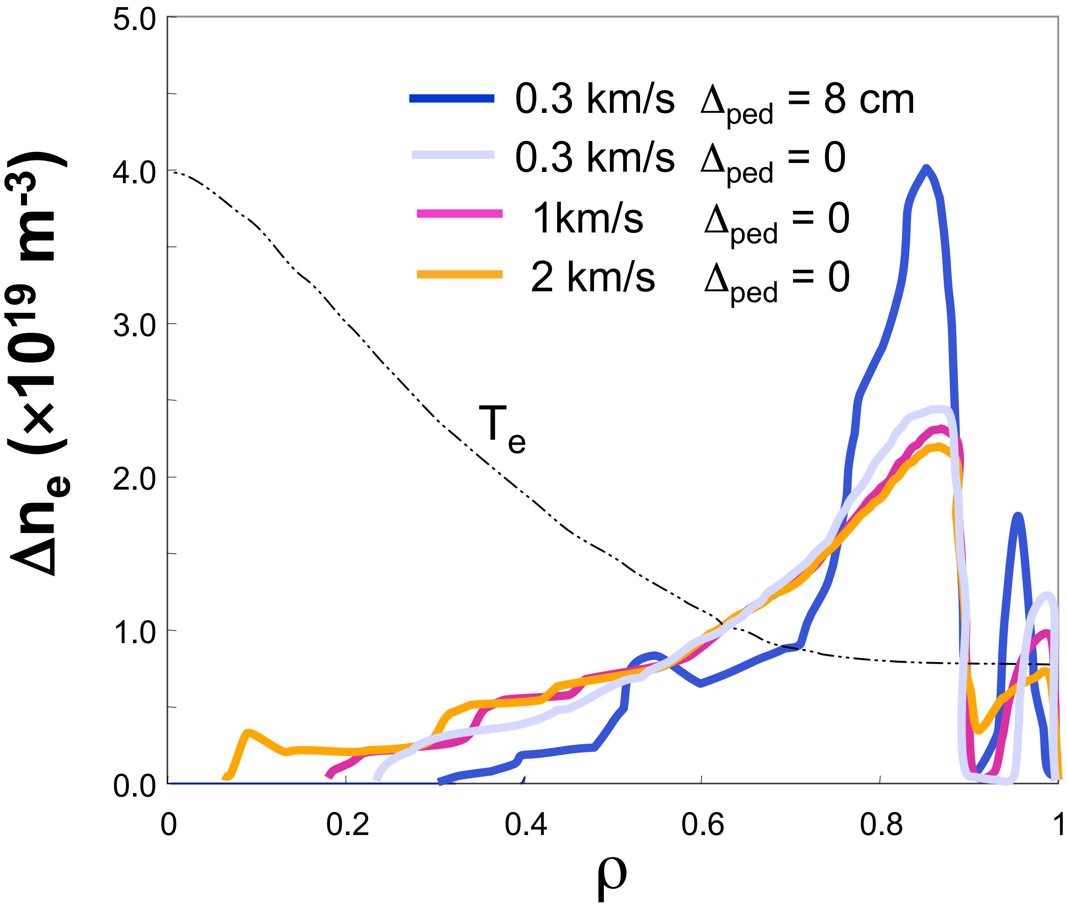

T_0 = 10 keV, T_{ped} = 4 keV
6 mm D_2

- ***Zero Pedestal width***
  - Pellet velocity makes scant difference in fuel deposition profile, because pellet penetration in a 4 keV edge plasma is poor anyway!
- ***Finite Pedestal width***
  - Higher velocity pays off: helps pellet punch through pedestal layer
  - → making higher pressure cloudlets, which drift further

ITER Deposition Profiles for Two Pellet Injection Scenarios

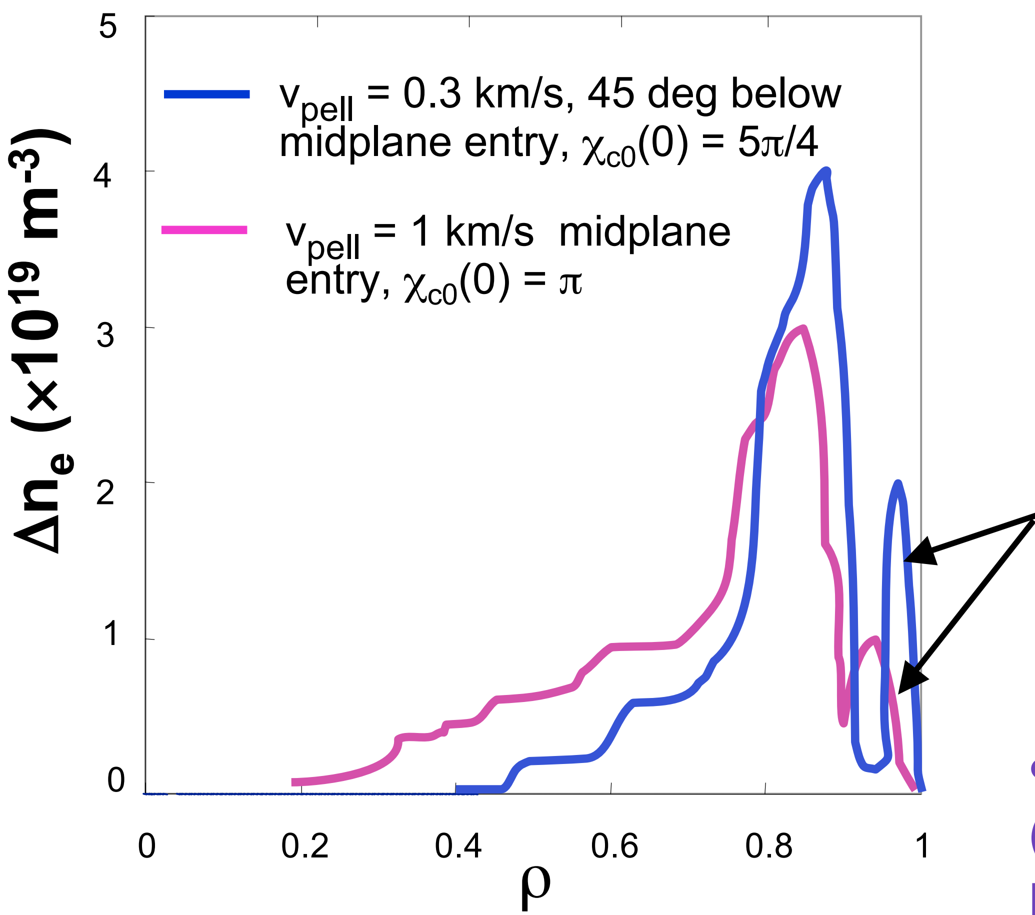

T_0 = 20 keV, T_{ped} = 4 keV

Δ_{ped} = 8 cm

6 mm D_2 pellet

q-profile with k = 5

10% of ablated material is assumed to be locally deposited (no drift)

- **A high-velocity inner-bore (midplane) pellet injector promotes deeper fueling (F.Perkins APS 2004) .**

ORNL OAK RIDGE NATIONAL LABORATORY

IAEA 2004

GENERAL ATOMICS

3-D AMR code: Numerical Approach and Assumptions

- Detailed 3D AMR simulations of pellet injection using the MHD equations– pellet treated as moving density source
  - Ratio of pellet size to device size is ~O(10^{-3})
- Phased approach to understand the basic physics of mass redistribution with varying degrees of complexity
  - Simple Cartesian geometry (Samtaney, Jardin, Colella and Martin, Sherwood Fusion Theory Conference 2003)
  - Toroidal geometry (ICNSP 2003 Invited talk. To appear in Comput. Phys. Comm.)
- Physical assumptions
  - Pellet ablation rate uses a semi-analytical model
  - Instantaneous heating of ablated mass by plasma electrons
    - Finite rate heating using kinetic model (Parks, PoP 2004) is in progress
  - Single fluid MHD equations describe plasma
  - Plasma pressure and B-field initialized by a Grad-Shafranov equilibrium solution → $p_\infty(\Psi)$, $T_\infty(\Psi)$, n_∞ = const

BERKELEY LAB

PPPL PRINCETON PLASMA PHYSICS LABORATORY

Equations and Mathematical Model

- Equations in conservation form + source terms

$$\frac{\partial U}{\partial t} + \frac{\partial F_j(U)}{\partial x_j} = \frac{\partial F_{v,j}(U)}{\partial x_j} + S_T(U) + S_{\nabla\cdot\mathbf{B}}(U) + S_{pellet}(U)$$

- Flux vector
  - *B_T is the toroidal component of the equilibrium magnetic field*

$$F_j(U) = \left\{ \begin{array}{c} \rho u_j \\ \rho u_i u_j + p_t \delta_{ij} - B_i B_j + B_T B_3 \delta_{ij} - B_i B_T \delta_{3j} - B_j B_T \delta_{i3} \\ u_j B_i - u_i B_j + B_T \delta_{i3} u_j - B_T \delta_{3j} u_i \\ (e + p + \frac{1}{2} B_k B_k) u_j - B_j (B_k u_k) + B_T B_3 u_j - (B_k u_k) B_T \delta_{3j} \end{array} \right\}$$

- Equation of state

$$e = \frac{p}{\gamma - 1} + \frac{\rho}{2} u_k u_k + \frac{1}{2} B_k B_k$$

Preliminary AMR Code Results Using NSTX Machine Parameters

— $n = 1.5 \times 10^{13}$ cm^{-3} , B = 0.23 T, a = 0.26 m, r_p= 1 mm, v_{pell} = 3200 m/s

Density iso-surface shows pellet cloud expanding along B-field

t/t_A=2

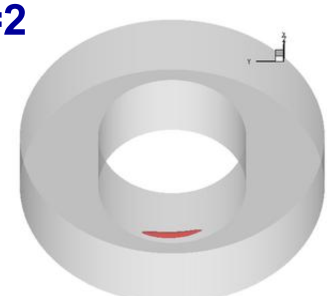

t/t_A= 20

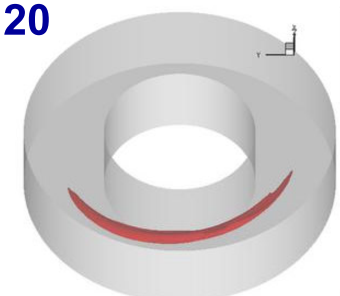

t/t_A= 60

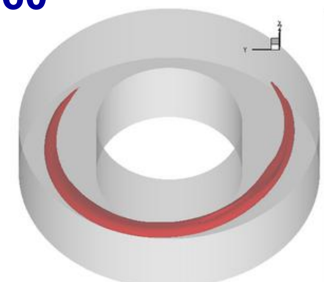

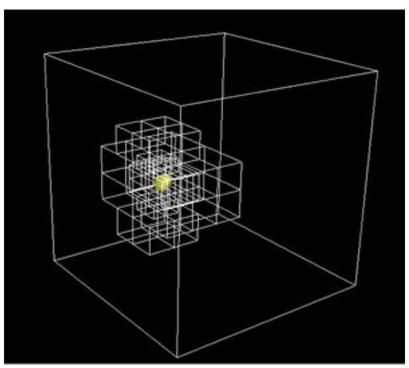

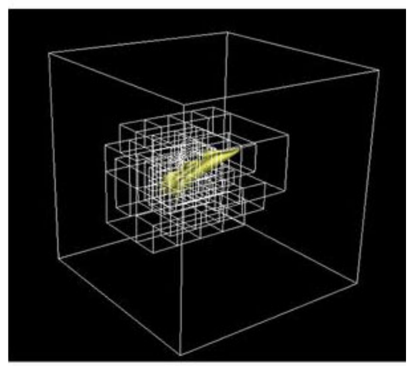

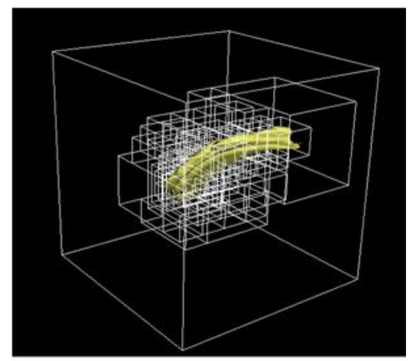

Adaptive Mesh Tracks Elongating Cloud

Inner Wall vs Outer Wall Pellet Injection (Midplane Entry)

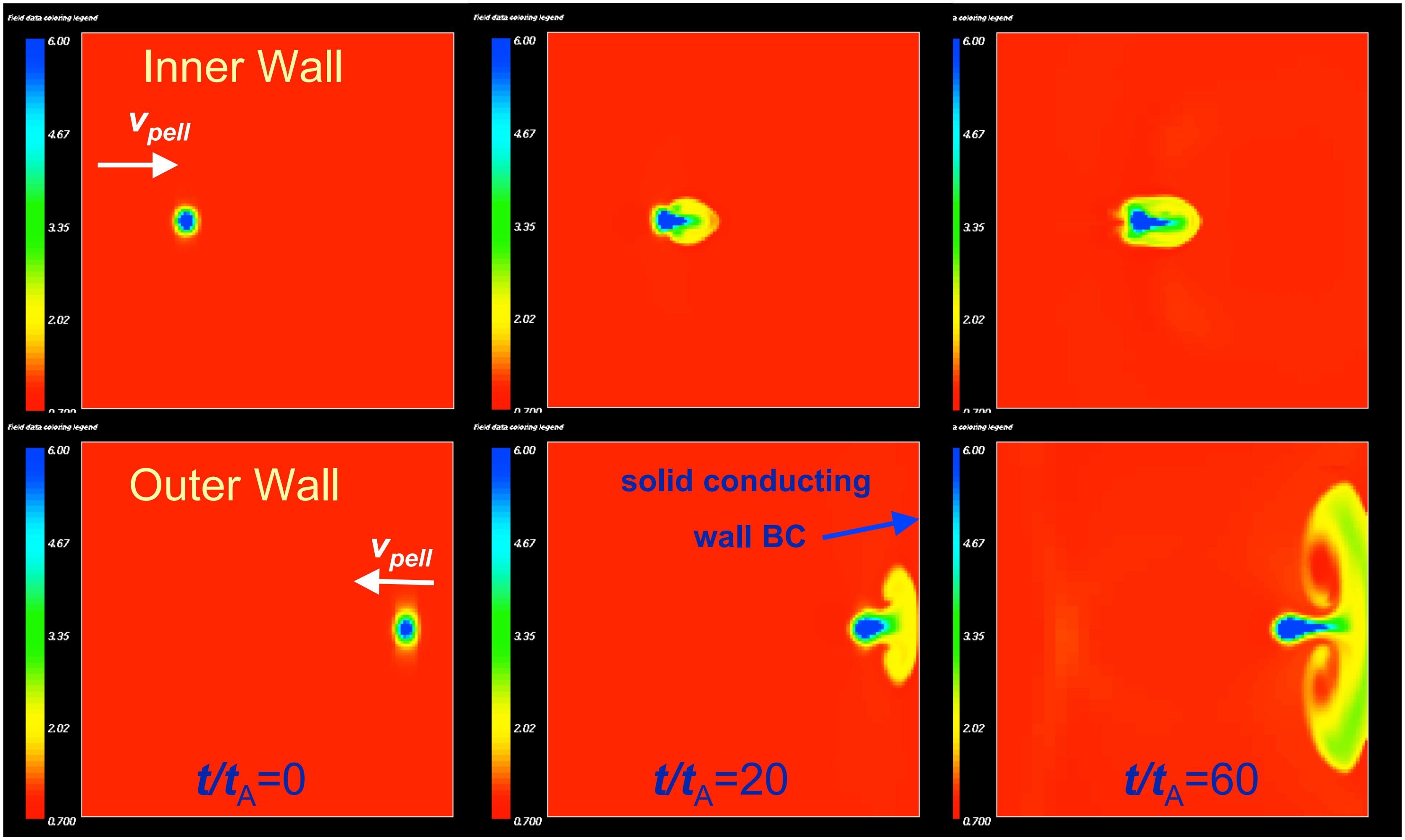

- Density contours of pellet cloud (at cloud midplane cross section) indicate significant large-*R* displacement relative to instantaneous pellet position.

Summary and Conclusions

- Pellet Ablation used 2-D **CAP** code, the most sophisticated ablation code which is now including the interaction of the ablation flow with the magnetic field
  - Showed that a $\beta \sim 1$ cavity can be formed around pellet by the high ablation pressure. This will reduce heat flux to pellet, but it contradicts previous quasi-steady ablation models in which *B*-field is only slightly distorted.
    - However **CAP** used a "switch-on" heat flux, described just the initial transient period to 0.4μs, and kept heat flux || to z, NOT DIVERTED AROUND B (which would reduce *p*,*T* and σ. "Switch-on" heat flux might apply to step-function high-T pedestal.
- The theoretical ∇B drift model has been reformulated with new physics
  - **PRL** code was validated by inner and outer wall pellet injection experiments on the DIII-D tokamak. Good agreement was found!
  - For ITER, **PRL** showed much better penetration of pellet material for inner wall injection, but penetration is sensitive to L_s, T_{ped}, and Δ_{ped}.
- 3-D numerical simulations of ∇B pellet cloud drift using **AMR** code are underway, verifying drift in the large-*R* direction for both inner- and outer-wall injection.